2.5 th Order Differential Electroanalysis

Masashi GOTO, Takafumi HIRANO, and Daido ISHII

Department of Applied Chemistry, Faculty of Engineering, Nagoya University, Chikusa-ku, Nagoya 464

(Received June 8, 1977)

The theory which describes the properties of the 2.5th order derivative of current, e'', *vs.* the electrode potential, E, curves is presented in response to an imposed ramp signal on a stationary electrode. The 2.5th order differential, $e''(t)$, of the current, $i(t)$, is defined by

$$e''(t) \equiv \frac{d^{2.5}}{dt^{2.5}} i(t) = \frac{d^3}{dt^3}\left[\frac{1}{\sqrt{\pi}}\int_0^t \frac{i(\lambda)}{\sqrt{t-\lambda}} d\lambda\right].$$

The predicted dependences of peak height, peak potential, and peak width on concentration, electron number, and scan rate, *etc.* have been confirmed experimentally, using the analogue circuit to monitor the electroreductions of Cd^{2+}, Pb^{2+}, Tl^{+}, Zn^{2+}, and Ni^{2+} on a hanging mercury electrode. It was proved that the proposed technique adds the advantages of further higher resolution and higher sensitivity to those of semidifferential electroanalysis. At the scan rate of 100 mV/s, the signals observed in this technique were about 50 and 8 times larger than those in linear sweep voltammetry for the reductions of Cd^{2+} and Ni^{2+}, respectively. Sufficient resolution was obtained for the qualitative analyses between Pb^{2+} and Tl^{+}, between Ni^{2+} and Zn^{2+}, and between Ni^{2+} and H^{+} at pH 1.4 in this technique.

Oscillographic polarography with applied voltage or, in other words, linear sweep voltammetry was first introduced by Matheson and Nichols[1] and developed by Randles[2] and Sevcik,[3] and many others[4] in order to reduce the time necessary for a polarographic analysis. In the linear sweep voltammetry, the electrolytic current increases up to a certain maximum value and then decreases rather gradually with increasing applied voltage. The maximum current, measured from the base line, is proportional to the bulk concentration of depolarizer, but it depends upon the potential scan rate and its constancy. The shape of the observed curve renders the determination of two or more depolarizers present very difficult. In 1972 Oldham[5-7] first introduced a new electroanalytical method "semiintegral electroanalysis" that has the merit of being independent of the details of the applied potential signal. The semiintegral, $m(t)$, of the current, $i(t)$, is defined by

$$m(t) \equiv \frac{d^{-0.5}}{dt^{-0.5}} i(t) = \frac{1}{\sqrt{\pi}}\int_0^t \frac{i(\lambda)}{\sqrt{t-\lambda}} d\lambda.$$

The method measures the semiintegral of the current as a function of electrode potential. When a ramp signal is applied, the shape of the observed curve is similar to that of a classical d.c. polarogram. Imbeux and Saveant,[8] and Senda and Ikeda[9] have also proposed, under the heading "convolutive potential sweep voltammetry," and "a new method for recording polarographic curves in oscillographic polarography with applied voltage, in which the surface concentration *vs.* potential curve is recorded," a similar transformation of the current *vs.* potential curve with reference to kinetic analysis of mechanisms and to analytical application, respectively.

By analogy with the relationship between d.c. polarography and a.c. polarography (or between normal pulse polarography and differential pulse polarography), a companion method "semidifferential electroanalysis" for semiintegral electroanalysis was recently announced by the present authors *et al.*[10-12] In this method, the semiderivative of current or the derivative of $m(t)$ is measured as a function of electrode potential, and the method appends the features of higher sensitivity and higher resolution to those of semiintegral electroanalysis as expected. For further higher resolution and higher sensitivity, the present article has proposed a new technique in which the 2.5th order derivative of current is recorded as a function of electrode potential.

Theory

Consider the case of a working electrode immersed in a solution containing, in addition to excess supporting electrolyte, a concentration C of the electroreducible species Ox. This species undergoes the n-electron reduction

$$Ox + ne^- \longrightarrow Rd \qquad (1)$$

to the initially-absent species Rd. A potential ramp,

$$E = E_0 - vt, \qquad (2)$$

is applied to the working electrode, where E is the electrode potential, E_0 is the initial potential, v is the scan rate of potential, and t is the time. E_0 is adjusted at a value at which Ox is virtually not reduced. It will be assumed throughout this article that the transport of Ox to, and of Rd in the reversible case from, the electrode is solely by semiinfinite diffusion.

We use the symbol e to denote the semiderivative[13] (0.5th order derivative) of the current i with respect to t

$$e \equiv \frac{d^{0.5}}{dt^{0.5}} i = \frac{d}{dt}\left[\frac{1}{\sqrt{\pi}}\int_0^t \frac{i(\lambda)}{\sqrt{t-\lambda}} d\lambda\right]. \qquad (3)$$

If Reaction 1 is reversible, the following equations[10]

$$e = \frac{nFv}{4RT} m_d \operatorname{sech}^2(x), \qquad (4)$$

where

$$m_d = nAF\sqrt{DC}\,, \qquad (5)$$

$$x = \frac{nF}{2RT}(E_{1/2} - E), \qquad (6)$$

relate the semiderivative of current to the electrode potential. In these equations, F is the Faraday constant, R is the gas constant, T is the absolute temperature, A is

the electrode area, D is the diffusion coefficient of Ox. and $E_{1/2}$ is the half-wave potential of the d.c. polarogram.

Differentiation of Eq. 4 with respect to t is aided by the chain rule in the form

$$e' \equiv \frac{de}{dt} = \frac{de}{dx}\cdot\frac{dx}{dt}, \tag{7}$$

and yields

$$e' \equiv \frac{d^{1.5}}{dt^{1.5}}i = -\left(\frac{nFv}{2RT}\right)^2 m_d \operatorname{sech}^2(x)\tanh(x), \tag{8}$$

as the expression for the shape of the 1.5th order derivative of current e' *vs.* E curve. On differentiation of Eq. 8, the 2.5th order derivative of current e'' is derived and presented by

$$e'' \equiv \frac{d^{2.5}}{dt^{2.5}}i = -\left(\frac{nFv}{2RT}\right)^3 m_d\{\operatorname{sech}^2(x) - 3\operatorname{sech}^2(x)\tanh^2(x)\}. \tag{9}$$

This equation represents the shape of a reversible e'' *vs.* E curve observed in the proposed method, to which the name "2.5th order differential electroanalysis" is suggested. The curve is symmetrical consisting of a minimum and two maxima as shown by the solid line in Fig. 1. The negative peak height is

$$e''_p = -m_d\left(\frac{nFv}{2RT}\right)^3, \tag{10}$$

and the potential corresponding to the negative peak is simply

$$E_p = E_{1/2}, \tag{11}$$

the polarographic half-wave potential. The width of the negative peak at an ordinate value equal to one-half of the peak height or, in short, the peak width is

$$W_p = \frac{1.56RT}{nF}. \tag{12}$$

Notice that the above peak width is much narrower than that of e *vs.* E curve which is $3.53\ RT/nF$.[11]

If Reaction 1 is totally irreversible, the following relation applies:[14]

$$e = -\frac{n\alpha Fv}{RT}m_d\sum_{j=1}^{\infty}\frac{(-1)^j j\exp(jz)}{\sqrt{j!}}, \tag{13}$$

where z is defined by

$$z = \frac{n\alpha F}{RT}(E_s - E) + \frac{1}{2}\ln\left(\frac{RTk_s^2}{n\alpha FvD}\right) \equiv \frac{n\alpha F}{RT}(E_* - E). \tag{14}$$

Here α is the transfer coefficient, E_s is the standard potential, k_s is the standard, heterogeneous rate constant, and E_* is a characteristic potential for an irreversible species being defined by Eq. 14. Differentiations of Eq. 13 with respect to t yield

$$e' = -\left(\frac{n\alpha Fv}{RT}\right)^2 m_d\sum_{j=1}^{\infty}\frac{(-1)^j j^2\exp(jz)}{\sqrt{j!}}, \tag{15}$$

and

$$e'' = -\left(\frac{n\alpha Fv}{RT}\right)^3 m_d\sum_{j=1}^{\infty}\frac{(-1)^j j^3\exp(jz)}{\sqrt{j!}}, \tag{16}$$

in the same way as for the reversible case. Equation 16 is the expression for the shape of a totally irreversible e'' *vs.* E curve observed in the proposed technique.

Values of the summation term in Eq. 16 for an assortment of small z values are listed in Table 1 together with the values of the hyperboric function term in Eq. 9 for x values. For large z values, sufficient precison of computation could not be retained. These data are also plotted as the dashed line in Fig. 1 for comparison with the corresponding shape of a reversible e'' *vs.* E curve. As expected, the irreversible peak is broader, and is somewhat asymmetric. From Table 1, the minimum value of the summation term is −0.2194, whence it follows that the negative peak height is

Table 1. Values of the function that describes the shapes of e'' *vs.* E curves

x, z	$-\{\operatorname{sech}^2(x) - 3\operatorname{sech}^2(x)\tanh^2(x)\}$	$-\sum_{j=1}^{\infty}(-1)^j j^3\exp(jz)/(j!)^{1/2}$
−2.50	0.0511	0.0495
−2.06	—	0.0553(b)
−2.00	0.1263	0.0551
−1.50	0.2634	0.0370
−1.15	0.3333(b)	—
−1.00	0.3108	−0.0276
−0.62(d)	—	−0.1097
−0.50	−0.2826	−0.1373
−0.39(c)	−0.5000	—
0.00	−1.0000(a)	−0.2177
0.07	—	−0.2194(a)
0.39(c)	−0.5000	—
0.50	−0.2826	−0.1606
0.67(d)	—	−0.1097
1.00	0.3108	−0.0049
1.15	0.3333(b)	—
1.20	—	0.0757
1.50	0.2634	
2.00	0.1263	
2.50	0.0511	

The entries marked (a) and (b) correspond to the negative and positive peaks of e'' *vs.* E curves, respectively, while those marked (c) and (d) correspond to the negative half-peak potentials of reversible and irreversible curves, respectively.

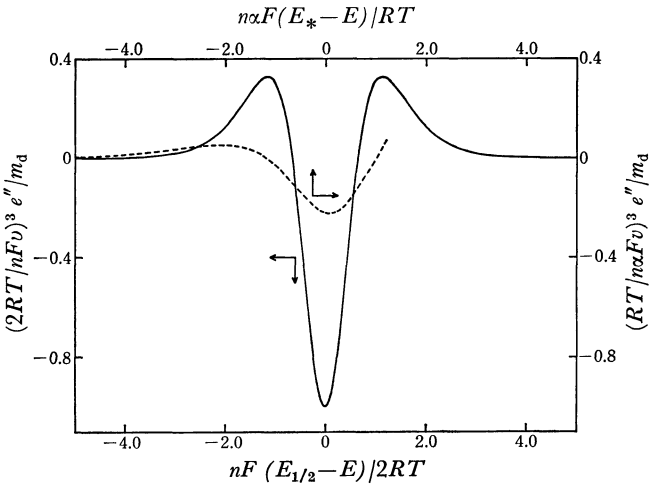

Fig. 1. Shapes of reversible (full line) and irreversible (dashed line) e'' *vs.* E curves.

$$e''_p = -0.219 m_d \left(\frac{n\alpha Fv}{RT}\right)^3. \quad (17)$$

From the fact that the minimum value of the summation occurs when z equals 0.07, if follows that the negative peak potential is

$$E_p = E_* - \frac{0.07RT}{n\alpha F}. \quad (18)$$

Likewise the tabulated data indicate the peak width to be

$$W_p = \frac{1.29RT}{n\alpha F}. \quad (19)$$

Information from Eqs. 10—12, 17—19 has been assembled into Table 2 which for 20 °C, summarizes the features of reversible and irreversible curves observed in the proposed technique.

Table 2. Features of e'' *vs.* E curves at 20 °C

	Reversible	Irreversible
Peak potential, E_p	$E_{1/2}$	$E_* - \frac{(1.77\text{ mV})}{n\alpha}$
Peak height, e''_p	$-\frac{n^4 A\sqrt{D}Cv^3}{(1.33n\text{ V}^3\text{ mol/C})}$	$-\frac{n^4\alpha A\sqrt{D}Cv^3}{(0.76n\text{ V}^3\text{ mol/C})}$
Peak width, W_p	$\frac{(39.4\text{ mV})}{n}$	$\frac{(32.5\text{ mV})}{n\alpha}$

The peak currents observed in linear sweep polarography[15] are given by

$$i_p = 0.447 m_d \left(\frac{nFv}{RT}\right)^{0.5}, \quad (20)$$

for reversible electrode processes, and

$$i_p = 0.496 m_d \left(\frac{n\alpha Fv}{RT}\right)^{0.5}, \quad (21)$$

for totally irreversible processes. Therefore the ratios of e''_p to i_p for reversible and irreversible processes are represented respectively by the following equations:

$$\frac{e''_p}{i_p} = -0.280 \left(\frac{nFv}{RT}\right)^{2.5}, \quad (22)$$

and

$$\frac{e''_p}{i_p} = -0.442 \left(\frac{n\alpha Fv}{RT}\right)^{2.5}. \quad (23)$$

The actual values of the ratios are listed in Table 3 for different potential scan rates, n and $n\alpha$ values at 20 °C. It is expected from Table 3 that the signals observed in this proposed method are further larger than those in linear sweep voltammetry at higher scan rates in both reversible and irreversible cases.

Table 3. Comparison of theoretical peak heights between e'' *vs.* E and i *vs.* E curves at 20 °C

v(V/s)	$-e''_p/i_p$ ($s^{-2.5}$) Reversible			Irreversible		
	$n=1$	$n=2$	$n=3$	$n\alpha=0.5$	$n\alpha=1$	$n\alpha=1.5$
0.05	1.54	8.74	24.1	0.429	2.44	6.72
0.10	8.74	49.4	136	2.44	13.8	38.0
0.20	49.4	280	770	13.8	78.0	215
0.50	488	2760	7610	136	771	2120
1.00	2760	15600	43100	771	4360	12000

Experimental

Apparatus. The instrument for 2.5th order differential electroanalysis was constructed from a function generator (NF Co., model FG-121B) as the applied potential sweeper, an analogue circuit for 2.5th order differential, and a recorder (Toa Electronics Ltd., model EPR-2TC). The 2.5th order differential circuit is shown in Fig. 2 with the circuit for correction of electrode sphericity effect. The current flowing through an indicator electrode is converted to voltage signal by means of a current follower (A1). The output of the current follower is fed to both a semidifferentiator (A2) and a potentiometer (PT). The potentiometer is adjusted to feed the voltage equivalent to $(\sqrt{D}/r)\,s^{1/2}$ portion of the output of the current follower to an adder (A3), where r is the radius of electrode sphere. The attenuated output of the current follower is subtracted from the output of the semidifferentiator by the adder. The output of the adder is fed to two differentiators (A4 and A5) in turn. When i, e', and e'' are to be recorded, the terminals of T1, T2, and T3 are connected directly to the recorder, respectively. Oldham's paralleling geometric ladder was used with a little modification as shown in Fig. 2 of the literature[16] as the semidifferential element (SE) in Fig. 2.

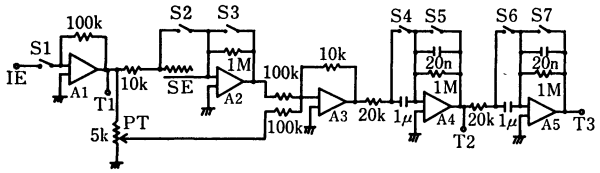

Fig. 2. 2.5th order differential circuit with the circuit for correction of electrode sphericity effect. IE: Indicator electrode, SE: semidifferential element, PT: potentiometer for the correction of electrode sphericity effect, S1: switch for electrolysis, S2—S7: switches for circuit reset, A1—A5: operational amplifiers (Analog Devices Co., model 118A), T1, T2, and T3: terminals for i, e', and e'' measurments, respectively.

A hanging mercury drop (Beckman Instruments Inc., model 39016) was used as a working electrode. A saturated calomel electrode with large surface area was served for both a counter and a reference electrode. A potential ramp signal was applied to the working electrode against the saturated calomel electrode.

Reagents etc. The salts $Cd(NO_3)_2 \cdot 4H_2O$, $Ni(NO_3)_2 \cdot 6H_2O$, $ZnSO_4 \cdot 7H_2O$, $TlNO_3$, and $Pb(NO_3)_2$ were used as solutes in 100 mmol/l KNO_3 plus HNO_3 at various concentrations. Solutions were prepared by direct weighing of the appropriate quantities of reagent grade chemicals, and deoxygenated by passage of N_2 gas. Measurments were made at room temperature (about 20 °C).

Results and Discussion

Figures 3 and 4 show typical e'' *vs.* E curves for Cd^{2+} as an example of reversibly reduced species and for Ni^{2+} as an example of irreversibly reduced ones, respectively, and also show the corresponding i *vs.* E and e' *vs.* E curves. As expected from the theory, a symmetric,

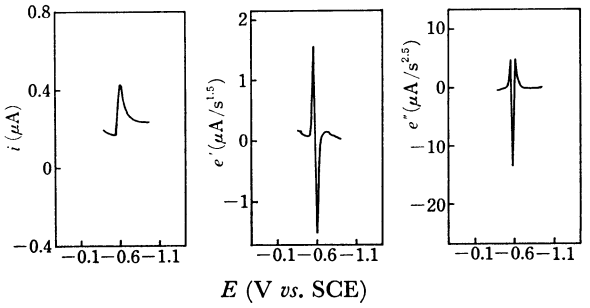

Fig. 3. Comparison of i *vs.* E, e' *vs.* E, and e'' *vs.* E curves of 10.5 μmol/l Cd^{2+} in 100 mmol/l KNO_3. Scan rate: 100 mV/s, electrode area: 4.69 mm^2.

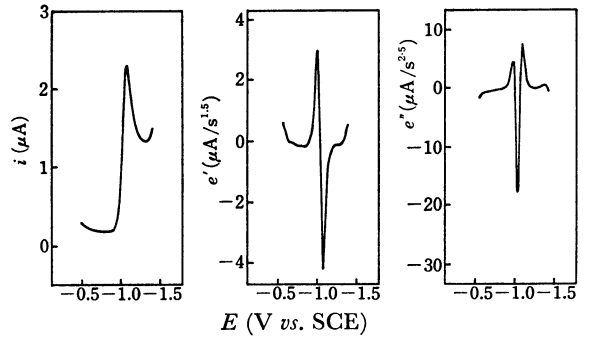

Fig. 4. Comparison of i *vs.* E, e' *vs.* E, and e'' *vs.* E curves of 104 μmol/l Ni^{2+} in 100 mmol/l KNO_3 plus 0.101 mmol/l HNO_3 (pH 4.1). Scan rate and electrode area: as Fig. 3.

sharp peak was observed in the e'' *vs.* E curve of Cd^{2+}, while a somewhat asymmetric, broad peak was observed in that of Ni^{2+}. It is evident from these diagrams that e'' *vs.* E and e' *vs.* E curves have attractive and promising features for both qualitative and quantitative analyses over ordinary i *vs.* E curve.

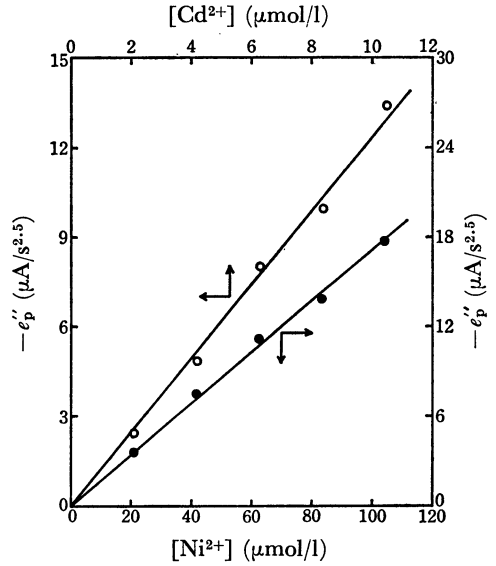

Fig. 5. Relationship between negative peak height of e'' *vs.* E curve and concentration of electroactive solutes. ○: Cd^{2+} in 100 mmol/l KNO_3, ●: Ni^{2+} in 100 mmol/l KNO_3 plus 0.101 mmol/l HNO_3, scan rate and electrode area: as Fig. 3.

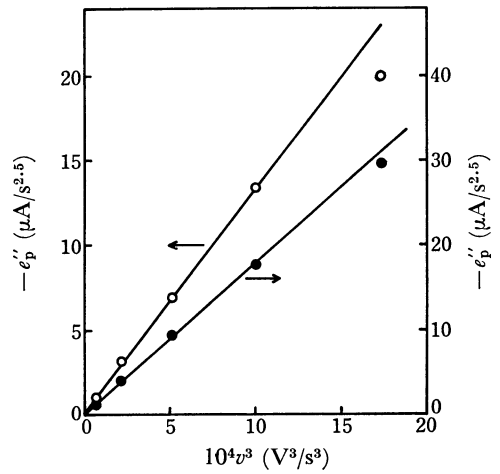

Fig. 6. Relationship between negative peak height of e'' *vs.* E curve and scan rate. ○: 10.5 μmol/l Cd^{2+} in 100 mmol/l KNO_3, ●: 104 μmol/l Ni^{2+} in 100 mmol/l KNO_3 plus 0.101 mmol/l HNO_3, electrode area: 4.69 mm^2.

Equations 5, 10, and 17 predict a linear dependence of negative peak height of e'' *vs.* E curve on the concentration of electroactive species and the cubic power of potential scan rate. These proportionalities are tested in Figs. 5 and 6 for Cd^{2+} and Ni^{2+} reductions, examples comprising both a reversible and an irreversible electrode reaction. In both cases, linearity was satisfactory and the lines passed through the origin. The slope de''_p/dC for Cd^{2+} in Fig. 5 has an experimental value of -1.24 A $s^{-2.5}$ mol^{-1} l, compared with a theoretical value, $-nAF\sqrt{D}(nFv/2RT)^3$, of -1.48 A $s^{-2.5}$ mol^{-1} l, calculated on the basis of a diffusion coefficient[17] of 6.9×10^{-6} cm^2 s^{-1}. Similarly for the Ni^{2+} line, the experimental slope $de''_p/dC=-0.170$ A $s^{-2.5}$ mol^{-1} l compares well with the theoretical value $-0.219nAF\sqrt{D}(n\alpha Fv/RT)^3=-0.166$ A $s^{-2.5}$ mol^{-1} l, based on $D=6.9\times10^{-6}$ cm^2 s^{-1} [18] and $\alpha=0.4$.[19] The slopes of the lines in Fig. 6 also agree approximately with the values predicted by Eqs. 10 and 17.

In Table 4 the experimental peak heights of e'' *vs.* E curves are compared with those of i *vs.* E curves at different concentrations for the Cd^{2+} and Ni^{2+} reductions. Table 4 also shows the corresponding, theoretical

Table 4. Comparison of experimental peak heights between e'' *vs.* E and i *vs.* E curves at the scan rate of 100 mV/s

Species	C (μmol/l)	i_p (μA)	e''_p (μA/$s^{2.5}$)	$-e''_p/i_p$($s^{-2.5}$) Exptl.	Theor.
Cd^{2+}	6.30	0.150	−8.09	53	49
Cd^{2+}	8.40	0.192	−9.96	52	49
Cd^{2+}	10.5	0.260	−13.4	52	49
Ni^{2+}	62.4	1.37	−11.2	8.2	7.9
Ni^{2+}	83.2	1.75	−13.8	7.9	7.9
Ni^{2+}	104	2.09	−17.7	8.5	7.9

Supporting electrolyte: 100 mmol/l KNO_3 for Cd^{2+}, 100 mmol/l KNO_3 plus 0.101 mmol/l HNO_3 for Ni^{2+}, electrode area: 4.69 mm^2.

Table 5. Peak potentials of e'' *vs.* E curves for Cd^{2+} and Ni^{2+} at different concentrations

$[Cd^{2+}]$ (μmol/l)	E_p for Cd^{2+} (mV *vs.* SCE)	$[Ni^{2+}]$ (μmol/l)	E_p for Ni^{2+} (mV *vs.* SCE)
2.10	−575	20.8	−1044
4.20	−586	41.6	−1048
6.30	−583	62.4	−1040
8.40	−587	83.2	−1046
10.5	−575	104	−1037
	Theor. −578[17]		Theor. −1034[18]

Supporting electrolyte, scan rate, and electrode area: as Table 4.

peak ratios of both curves for reference. It is evident from Table 4 that at the scan rate of 100 mV/s, the proposed technique provides about 50 and 8 times larger signals for Cd^{2+} and Ni^{2+} reductions, respectively, than linear sweep voltammetry does.

The peak potentials of e'' *vs.* E curves for the reductions of Cd^{2+} and Ni^{2+} were found to be independent of concentration, as shown in Table 5, and to average respectively −581 and −1043 mV *vs.* SCE (the latter value refers to $v=100$ mV/s). The experimental peak potential for Cd^{2+} is to be compared with the polarographic half-wave potential in the literature[17] of −578 mV *vs.* SCE. That for Ni^{2+} may likewise be compared with the −1034 mV *vs.* SCE value calculated from the half-wave potential of −980 mV *vs.* SCE at the mercury drop time τ of 4.48 s in classical polarography[18] by application of Eq. 18 and the relation[11]

$$E_{1/2} = E_* + \frac{0.30RT}{n\alpha F} + \frac{RT}{2n\alpha F} \ln\left(\frac{n\alpha Fv\tau}{RT}\right). \quad (24)$$

For Ni^{2+} reduction, the peak potential should vary with scan rate in accordance with the relation:

$$E_p = E_s + \frac{RT}{2n\alpha F} \ln\left(\frac{0.869RTk_s^2}{n\alpha FD}\right) - \frac{RT}{2n\alpha F} \ln(v)$$

predicted by Eqs. 14 and 18, while it should be independent of scan rate for Cd^{2+} reduction. Table 6 resorts the experimental data and lists the theoretical values of peak potentials. Agreement is within a few millivolts in all the cases.

Table 7 assesses how well the observed peak widths in the proposed technique agree with theoretical predictions. The data refer to the reduction of Cd^{2+} and Ni^{2+}

Table 6. Scan rate dependence of peak potentials of e'' *vs.* E curves for Cd^{2+} and Ni^{2+}

v (mV/s)	E_p for Cd^{2+} (mV *vs.* SCE)		E_p for Ni^{2+} (mV *vs.* SCE)	
	Exptl.	Theor.	Exptl.	Theor.
20	−576	−578	−1015	−1008
40	−573	−578	−1023	−1019
60	−571	−578	−1028	−1026
80	−572	−578	−1030	−1030
100	−575	−578	−1037	−1034
120	−574	−578	−1041	−1036

Supporting electrolyte and electrode area: as Table 4, electroactive concentration: 10.5 μmol/l for Cd^{2+}, 104 μmol/l for Ni^{2+}.

Table 7. Peak width values of e'' *vs.* E curves for Cd^{2+} and Ni^{2+}

C (μmol/l)	v (mV/s)	W_p for Cd^{2+} (mV)		W_p for Ni^{2+} (mV)	
		Exptl.	Theor.	Exptl.	Theor.
8.40	100	24	20		
10.5	100	22	20		
20.8	100			42	41
41.6	100			39	41
62.4	100			41	41
10.5	20	22	20		
10.5	60	24	20		
10.5	80	23	20		
104	20			41	41
104	60			41	41
104	100			42	41

Supporting electrolyte and electrode area: as Table 4.

as an example of reversible and irreversible processes, respectively. The theoretical predictions are based on Eqs. 12 and 19.

All theoretical predictions concerning 2.5th order differential electroanalysis have been confirmed. Though this entire article is couched in terms of cathodic processes, it is evident that the conclusions are easily widened to embrace electrooxidations.

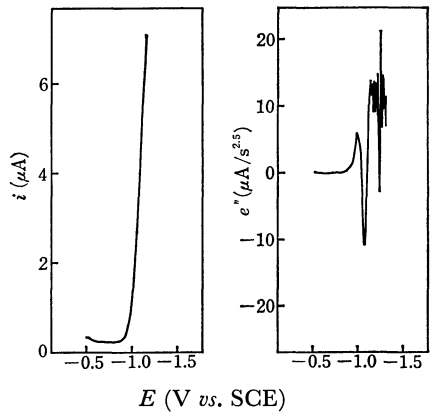

Fig. 7. Comparison of resolution between i *vs.* E and e'' *vs.* E curves for 104 μmol/l Ni^{2+} plus 50.5 mmol/l H^+ in 100 mmol/l KNO_3. Scan rate and electrode area: as Fig. 3.

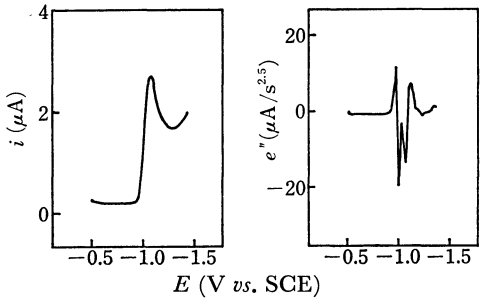

Fig. 8. Comparison of resolution between i *vs.* E and e'' *vs.* E curves for 25.0 μmol/l Zn^{2+} plus 104 μmol/l Ni^{2+} in 100 mmol/l KNO_3 plus 0.101 mmol/l HNO_3. Scan rate and electrode area: as Fig. 3.

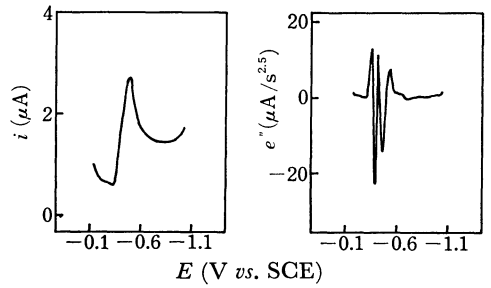

Fig. 9. Comparison of resolution between i *vs.* E and e'' *vs.* E curves for 20.0 μmol/l Pb^{2+} plus 100 μmol/l Tl^{+} in 100 mmol/l KNO_3 plus 10.1 mmol/l HNO_3. Scan rate and electrode area: as Fig. 3.

Figures 7, 8, and 9 demonstrate how clear resolution the proposed technique provides by comparison with ordinary linear sweep voltammetry. It is evident from these diagrams that Ni^{2+} in 100 mmol/l KNO_3 at pH 1.4 can be detected separately from hydrogen wave and simultaneous detections between Zn^{2+} and Ni^{2+}, and between Pb^{2+} and Tl^{+}, whose reduction potentials close together, are possible in the proposed technique.

In conclusion, 2.5th order differential electroanalysis is an attractive, fast method for the identification of many electroactive species coexistent in solution, and may provide quite high sensitivity for the detection of electroactive species at higher scan rates of potential as expected from Table 3. The study of detection limit for various species in this technique is continuing in our laboratory.

The authors are grateful to Dr. T. Matsuzaki and Mr. K. Kitagawa, Nagoya University, for computational assistance.

References

1) L. A. Matheson and N. Nichols, *Trans. Electrochem. Soc.*, **73**, 193 (1938).
2) J. E. B. Randles, *Trans. Faraday Soc.*, **44**, 3241 (1950).
3) A. Sevcik, *Coll. Czech. Chem. Commun.*, **13**, 349 (1948).
4) S. P. Perone, D. O. Jones, and W. F. Gutknecht, *Anal. Chem.*, **41**, 1154 (1969).
5) K. B. Oldham, *Anal. Chem.*, **44**, 196 (1972).
6) M. Grenness and K. B. Oldham, *Anal. Chem.*, **44**, 1121 (1972).
7) M. Goto and K. B. Oldham, *Anal. Chem.*, **45**, 2043 (1973).
8) J. C. Imbeux and J. M. Saveant, *J. Electroanal. Chem.*, **44**, 169 (1973).
9) M. Senda and T. Ikeda, *Rev. Polarogh. (Kyoto)*, **19**, 51 (1973).
10) M. Goto and D. Ishii, *J. Electroanal. Chem.*, **61**, 361 (1975).
11) P. Dalrymple-Alford, M. Goto, and K. B. Oldham, *J. Electroanal. Chem.*, **85**, 1 (1977).
12) P. Dalrymple-Alford, M. Goto, and K. B. Oldham, *Anal. Chem.*, **49**, 1390 (1977).
13) K. B. Oldham and T. Spanier, "The Fractional Calculus," Academic Press, New York (1974), p. 115.
14) M. Goto and K. B. Oldham, *Anal. Chem.*, **48**, 1671 (1976).
15) H. Matsuda and Y. Ayabe, *Z. Elektrochem.*, **59**, 494 (1955).
16) M. Goto, M. Kato, and D. Ishii, *Nippon Kagaku Kaishi*, **1977**, 42.
17) J. Heyrovsky and J. Kuta, "Principles of Polarography," Academic Press, New York (1965), pp. 106, 534.
18) P. Kivalo, K. B. Oldham, and H. A. Laitinen, *J. Am. Chem. Soc.*, **75**, 4148 (1953).
19) N. Tanaka and R. Tamamushi, *Electrochim. Acta*, **9**, 963 (1964).